

## **Chapter 6 – Stability of Finite-Difference Time-Domain (FDTD) Method with Nonlinear Lumped Elements**

### **6.1 Introduction**

Traditionally to ensure numerical stability of the algorithm for a linear model, the Courant-Friedrich-Lewy (CFL) Criterion (3.5.2) has to be fulfilled (Taflove 1995). In an unstable algorithm the computed E and H field components will increase without limit as the simulation progresses. The CFL Criterion has been derived with the assumption of homogeneous linear dielectric and unbounded medium using Discrete Fourier Transform (DFT) (the Von Neumann approach, see Appendix 2). For a practical microwave circuit model the CFL Criterion serves as a rule-of-thumb at best. A few attempts recently extended the stability analysis to include linear dispersive media (Pereda et.al 2001) and linear lumped elements (Thiel and Katehi, 2002). There is also an attempt to cast the FDTD method into iterative matrix equation (Remis 2000). The methods reported still rely on mathematical tools for linear systems (i.e. superposition principle, DFT etc.) and will fail for nonlinear models. To-date, to the best of the author's knowledge, there is still no satisfactory theory to explain the stability of FDTD formulation containing non-homogeneous dielectrics, boundary condition, nonlinear dielectric and also linear and nonlinear lumped elements arranged in an arbitrary manner. In this chapter new stability theorems based on the energy method are derived to address the issue. This work is inspired by stability theory of dynamical systems (Scheinerman 1996), notably the Second Liapunov Method (Elaydi 2000, Merkin 1997, Khalil 1996). Although not shown due to lack of space, the FDTD formulation is actually a discrete dynamical system. The proofs of the new theorems are shown in Appendix 3 to Appendix 6 and the application is demonstrated in the main text. The theorems are used to prove what have been known throughout the years via simulation, that the incorporation of certain lumped components such as resistor, capacitor, diode and bipolar junction transistor in the FDTD framework is found to be stable. The theorems also show with ease how a model containing non-homogeneous and nonlinear dielectric is stable. The theorems are intended to complement the CFL

Criterion and the results of Pereda et al. (2001), Thiel and Katehi (2002) and Remis (2000). In Section 6.3 it is shown how the theorems are used as a test, to determine whether the inclusion of new lumped element in FDTD is proper without performing lengthy simulation. A proper formulation will preserve the stability of the FDTD model. This chapter begins by considering a 3D FDTD model for PCB or microwave circuit without any source (voltage or current source), with perfect electric conductor (PEC) as the model boundaries. The new theorems are stated and are used to prove the stability of the sourceless model. Then the theorems are extended to check the stability of a 3D FDTD model with a resistive voltage source. A simple simulation example serves to substantiate the results. Finally, extension of the theorems to a three-dimensional PCB model with absorbing boundary conditions (ABCs) is shown in Appendix 6.

## 6.2 The New Stability Theorems

Figure 6.1 shows a typical 3D FDTD model for microwave circuit PCB without any voltage or current source, with perfect electric conductor (PEC) as the model boundaries. The model has  $n_x$ ,  $n_y$  and  $n_z$  cells along x, y and z axis respectively. The model is assumed to be non-magnetic, i.e.  $\mu = \mu_0$  for all H fields. Also the cells are the same in size. All the E and H field components within the model have update equations given by the following form (as can be seen from Section 4.3 and Section 4.4):

$$H_{x(i,j,k)}^{n+\frac{1}{2}} = H_{x(i,j,k)}^{n-\frac{1}{2}} - \frac{\Delta t}{\mu} \nabla \times E_{x(i,j,k)}^n \quad (6.2.1a)$$

$$H_{y(i,j,k)}^{n+\frac{1}{2}} = H_{y(i,j,k)}^{n-\frac{1}{2}} - \frac{\Delta t}{\mu} \nabla \times E_{y(i,j,k)}^n \quad (6.2.1b)$$

$$H_{z(i,j,k)}^{n+\frac{1}{2}} = H_{z(i,j,k)}^{n-\frac{1}{2}} - \frac{\Delta t}{\mu} \nabla \times E_{z(i,j,k)}^n \quad (6.2.1c)$$

$$E_{x(i,j,k)}^{n+1} = E_{x(i,j,k)}^n + \frac{\Delta t}{\epsilon_{x(i,j,k)}} \left[ \nabla \times H_{x(i,j,k)}^{n+\frac{1}{2}} - J_{x(i,j,k)}^{n+\frac{1}{2}} \right] \quad (6.2.1d)$$

$$E_{y(i,j,k)}^{n+1} = E_{y(i,j,k)}^n + \frac{\Delta t}{\epsilon_{y(i,j,k)}} \left[ \nabla \times H_{y(i,j,k)}^{n+\frac{1}{2}} - J_{y(i,j,k)}^{n+\frac{1}{2}} \right] \quad (6.2.1e)$$

$$E_{z(i,j,k)}^{n+1} = E_{z(i,j,k)}^n + \frac{\Delta t}{\epsilon_{z(i,j,k)}} \left[ \nabla \times H_{z(i,j,k)}^{n+\frac{1}{2}} - J_{z(i,j,k)}^{n+\frac{1}{2}} \right] \quad (6.2.1f)$$

Where in (6.2.1a)-(6.2.1f),

$$\nabla \times E_{x(i,j,k)}^n = \frac{E_{z(i,j+1,k)}^n - E_{z(i,j,k)}^n}{\Delta y} - \frac{E_{y(i,j,k+1)}^n - E_{y(i,j,k)}^n}{\Delta z} \quad (6.2.1g)$$

$$\nabla \times H_{x(i,j,k)}^{n+\frac{1}{2}} = \frac{H_{z(i,j,k)}^{n+\frac{1}{2}} - H_{z(i,j-1,k)}^{n+\frac{1}{2}}}{\Delta y} - \frac{H_{y(i,j,k)}^{n+\frac{1}{2}} - H_{y(i,j,k-1)}^{n+\frac{1}{2}}}{\Delta z} \quad (6.2.1h)$$

and so forth for y and z terms. Notice that the restriction for  $\epsilon$  has been removed, allowing it to vary according to location and orientation. Though not indicated,  $\epsilon_{r(i,j,k)}$  ( $r = x, y, z$ ) can also be functions of field components. Similarly the current density term  $J_{r(i,j,k)}^{n+\frac{1}{2}}$  ( $r = x, y, z$ ) also depends only on E field components at earlier time-steps.

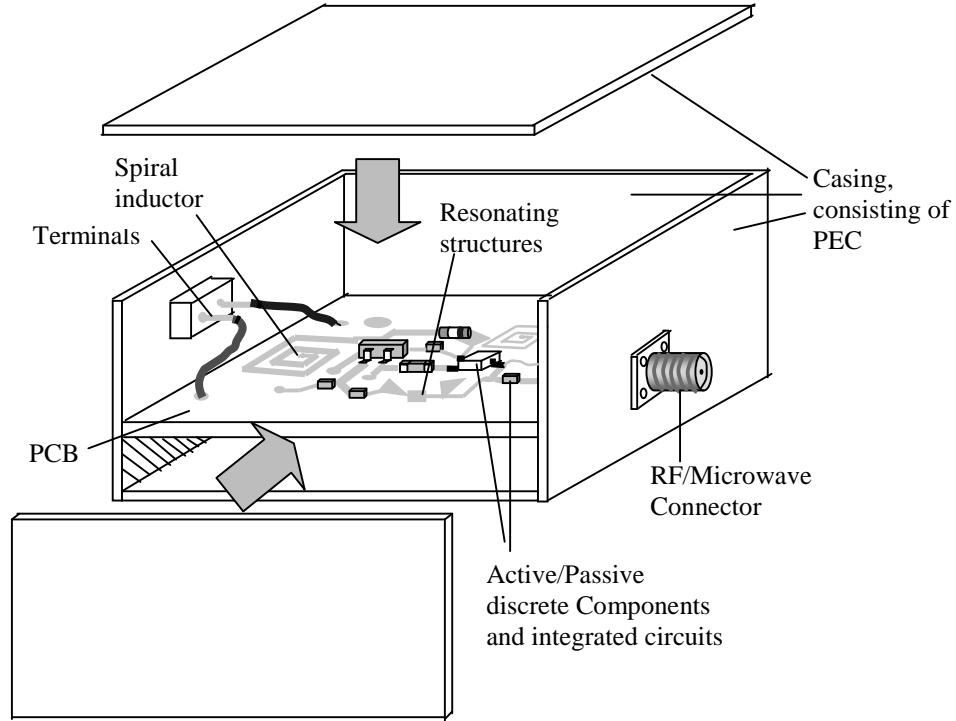


**Figure 6.1** – A typical microwave circuit module.

Equations (6.2.1a)-(6.2.1f) will be known as the *Canonical FDTD Form* for E and H field components. Update equations for many applications can usually be written in this form. Let us now introduce two new quantities, as defined by:

$$\mathbf{V}^n = \frac{\Delta V}{2} \sum_{k=1}^{n_z} \sum_{j=1}^{n_y} \sum_{i=1}^{n_x} \left[ \begin{array}{l} \sum_{r=x,y,z} \left( \epsilon_{r(i,j,k)} (E_{r(i,j,k)}^n)^2 + \mu_o (H_{r(i,j,k)}^{n-\frac{1}{2}})^2 \right) \\ - H_{x(i,j,k)}^{n-\frac{1}{2}} \left[ \frac{\Delta t}{\Delta y} (E_{z(i,j+1,k)}^n - E_{z(i,j,k)}^n) - \frac{\Delta t}{\Delta z} (E_{y(i,j,k+1)}^n - E_{y(i,j,k)}^n) \right] \\ - H_{y(i,j,k)}^{n-\frac{1}{2}} \left[ \frac{\Delta t}{\Delta z} (E_{x(i,j,k+1)}^n - E_{x(i,j,k)}^n) - \frac{\Delta t}{\Delta x} (E_{z(i+1,j,k)}^n - E_{z(i,j,k)}^n) \right] \\ - H_{z(i,j,k)}^{n-\frac{1}{2}} \left[ \frac{\Delta t}{\Delta x} (E_{y(i+1,j,k)}^n - E_{y(i,j,k)}^n) - \frac{\Delta t}{\Delta y} (E_{x(i,j+1,k)}^n - E_{x(i,j,k)}^n) \right] \end{array} \right] \quad (6.2.2a)$$

$$P_d = -\Delta V \sum_{k=1}^{n_z} \sum_{j=1}^{n_y} \sum_{i=1}^{n_x} \left\{ \sum_{r=x,y,z} \frac{1}{2} (E_{r(i,j,k)}^{n+1} + E_{r(i,j,k)}^n) J_{r(i,j,k)}^{n+\frac{1}{2}} \right\} \quad (6.2.2b)$$

where  $\Delta V = \Delta x \Delta y \Delta z$ . In equation (6.2.2a),  $\mathbf{V}^n$  is known as the ‘numerical energy’ of the 3D FDTD model at sequence  $n$ , it is analogous to the stored electromagnetic energy in a physical system. It comprises all the E field components at time-step  $n$  and H field components at time-step  $n - \frac{1}{2}$ . Similarly the numerical energy  $\mathbf{V}^{n+1}$  comprises all E and H field components at time-steps  $n+1$  and  $n + \frac{1}{2}$  respectively. In (6.2.2b) each term

$\frac{1}{2} (E_{r(i,j,k)}^{n+1} + E_{r(i,j,k)}^n) J_{r(i,j,k)}^{n+\frac{1}{2}}$  will be known as ‘elemental dissipation’ since it is the approximate power density dissipated by lumped element coinciding with  $E_{r(i,j,k)}$  field. The negative sum of all elemental dissipation multiplied by  $\Delta V$  is the total dissipation  $P_d$  of the model. Since all the boundaries are PEC, the numerical energy within the model cannot escape from the boundary. The following theorems give the relationship between numerical energy and total dissipation, and the stability result.

Lemma 6.1 – Relationship between numerical energy and total dissipation

Consider a 3D FDTD model with PEC boundaries of Figure 6.1. Given that all field update equations are of the form (6.2.1a)-(6.2.1f), with  $V^n$  and  $P_d$  as defined in (6.2.2a) and (6.2.2b), then the following relation is true:

$$V^{n+1} - V^n = \Delta t \cdot P_d \quad (6.2.3)$$

Lemma 6.2 – Positive semi-definiteness of  $V^n$

Consider a 3D FDTD model with PEC boundaries of Figure 6.1. Given that all field update equations are of the form (6.2.1a)-(6.2.1f), then  $V^n$  is positive definite if and only if:

$$(a) \quad \varepsilon_{x(i,j,k)} > 0, \varepsilon_{y(i,j,k)} > 0, \varepsilon_{z(i,j,k)} > 0 \text{ and } \mu = \mu_o > 0. \quad (6.2.4a)$$

$$(b) \quad \text{For } \varepsilon = \min\{\varepsilon_{x(i,j,k)}, \varepsilon_{y(i,j,k)}, \varepsilon_{z(i,j,k)}\} \text{ and } c_m = \frac{1}{\sqrt{\mu_o \varepsilon}}, \text{ let:}$$

$$\Delta t < \min \left\{ \frac{1}{c_m \sqrt{2} \sqrt{\frac{1}{\Delta y^2} + \frac{1}{\Delta z^2}}}, \frac{1}{c_m \sqrt{2} \sqrt{\frac{1}{\Delta x^2} + \frac{1}{\Delta z^2}}}, \frac{1}{c_m \sqrt{2} \sqrt{\frac{1}{\Delta x^2} + \frac{1}{\Delta y^2}}} \right\} \quad (6.2.4b)$$

where  $i \in \{1, 2, \dots, n_x\}$ ,  $j \in \{1, 2, \dots, n_y\}$ ,  $k \in \{1, 2, \dots, n_z\}$ .

A function  $f(x)$  is positive definite when  $x \neq 0$  implies  $f(x) > 0$ , and  $f(x) = 0$  when  $x = 0$  (Khalil 1996). Note that  $x$  can be a vector or a scalar. The proofs for Lemma 6.1 and Lemma 6.2 are shown in Appendix 3. In this context stability implies the FDTD algorithm for the 3D model is both numerically and dynamically stable. This means that if we were to reduce  $\Delta t$  to zero or increase the time-step  $n$  to infinity, the solution for E and H field components would always remain bounded. The definition for stability of the 3D FDTD model is quite similar to Definition 2.2. It will be defined again in the context of the FDTD algorithm in E and H field components.

Definition 6.1 – Stability of FDTD algorithm

Suppose we construct a vector  $\bar{X}^n$  whose elements consist of all E and H field components of the model:

$$\bar{X}^n = \begin{bmatrix} E_{x(1,1,1)}^n \\ E_{x(2,1,1)}^n \\ \vdots \\ E_{z(n_x+1,n_y+1,n_z)}^n \\ H_{x(1,1,1)}^{n-\frac{1}{2}} \\ H_{x(2,1,1)}^{n-\frac{1}{2}} \\ \vdots \\ H_{z(n_x,n_y,n_z+1)}^{n-\frac{1}{2}} \end{bmatrix} \quad (6.2.5a)$$

$$\dim \bar{X}^n = M = 6n_x n_y n_z + 3(n_x n_y + n_x n_z + n_y n_z) + n_x + n_y + n_z \quad (6.2.5b)$$

Then the FDTD algorithm is stable when

$$\|\bar{X}^n\| \leq C(T) \quad n = 1, 2, 3, \dots, N \quad (6.2.5c)$$

The symbol  $\|\bar{x}\|$  means taking the ‘norm’ of a vector  $\bar{x}$  (Ortega 1987), which is a measure of the ‘distance’ between  $\bar{x}$  and the origin.  $C(T)$  is a positive real value which depends only on  $T$ , the maximum computation time.  $N = T / \Delta t$  is the maximum sequence. As  $\Delta t \rightarrow 0$ ,  $N$  will approach infinity. However (6.2.5c) dictates that  $C(T)$  must be finite as  $N$  approaches infinity as long as  $T$  is bounded. We allow  $C$  to be a function of  $T$  as certain solution of the FDTD can increase with time. For instance when there is a source in the model that increases with time, it is then reasonable to expect the field components to gradually increase too. What (6.2.5c) means is that the solution remains bounded for finite time interval. If (6.2.5c) is not fulfilled as  $n$  increases, then the algorithm is not stable. Finally we define the stability theorem:

### Theorem 6.3 – Stability theorem for 3D FDTD model

Consider a 3D FDTD model with PEC boundaries of Figure 6.1, if the model fulfills all the conditions in Lemma 6.2, then a sufficient condition for it to be stable is  $P_d \leq 0$ .

The proof is given in Appendix 4. The next section will show how Lemma 6.1, Lemma 6.2 and Theorem 6.3 can be used to determine the stability of a general 3D FDTD model for microwave circuits.

### **6.3 Application Example – Establishing the Stability of a Sourceless 3D Printed Circuit Board (PCB) Model**

Assume a PCB model of Figure 6.1. The PCB model contains non-homogeneous dielectric, lumped resistors, lumped capacitors and nonlinear components such as PN junctions and bipolar junction transistors (BJTs). The FDTD update equations for E and H fields of all these elements can be found in Section 4.3 and Section 4.4. Initially only a sourceless 3D FDTD model will be considered for reasons to be explained in Section 6.4. This means the model will not contain any source, such as the lumped resistive voltage source (equation (4.3.6)). The analysis begins by computing the elemental dissipation  $\frac{1}{2} \left( E_{r(i,j,k)}^{n+1} + E_{r(i,j,k)}^n \right) J_{r(i,j,k)}^{n+\frac{1}{2}}$  of each element, and show that this is always greater or equal to zero under normal E and H field values. Furthermore it will also be shown that  $\epsilon_{r(i,j,k)}$  is always positive under normal field values. Element meeting these two characteristics is called proper. An elemental dissipation  $> 0$  means that the element is absorbing numerical energy from the model. When all the elements are proper, the total dissipation  $P_d$  will be equal to zero or negative. If  $V^n$  is positive definite, the condition of Theorem 6.3 will be fulfilled. The time discretization  $\Delta t$  is as dictated by (6.2.4b) of Lemma 6.2. With the final condition met, Theorem 6.3 tells us that the model will be stable. For simplicity it is assumed the elements are oriented in the +z direction. This can always be generalized to elements oriented along other directions.

### Lossless Linear Dielectric

For the  $E_z$  field of a lossless linear dielectric (3.3.4f):

$$E_{z(i,j,k)}^{n+1} = E_{z(i,j,k)}^n + \frac{\Delta t}{\epsilon_r \epsilon_o} \nabla \times H_{z(i,j,k)}^{n+\frac{1}{2}} \quad (6.3.1a)$$

where  $\nabla \times H_{z(i,j,k)}^{n+\frac{1}{2}}$  is as defined in (6.2.1h). Comparing (6.3.1a) with the Canonical

FDTD Form for  $E_z$  component:

$$J_{z(i,j,k)}^{n+\frac{1}{2}} = 0 \quad \text{and} \quad \epsilon_{z(i,j,k)} = \epsilon_r \epsilon_o \quad (6.3.1b)$$

Thus elemental dissipation  $\frac{1}{2} (E_{z(i,j,k)}^{n+1} + E_{z(i,j,k)}^n) J_{z(i,j,k)}^{n+\frac{1}{2}} = 0$ . Since  $\epsilon_{z(i,j,k)} = \epsilon_r \epsilon_o > 0$ , the lossless linear dielectric formulation is proper.

### Perfect Electric Conductor (PEC)

The electric field in a PEC is always 0. It can be written as:

$$E_{z(i,j,k)}^{n+1} = 0 = E_{z(i,j,k)}^n + \frac{\Delta t}{\epsilon_{PEC}} \nabla \times H_{z(i,j,k)}^{n+\frac{1}{2}} \quad (6.3.2)$$

where  $\epsilon_{PEC} \rightarrow +\infty$ , assuming  $E_{z(i,j,k)}^0 = 0$ . Again comparison with Canonical FDTD

Form shows that  $J_{z(i,j,k)}^{n+\frac{1}{2}} = 0$ , implying elemental dissipation is 0. The PEC formulation is proper.

### Capacitor

For a lumped capacitor C oriented in z axis, according to (4.3.8):

$$\begin{aligned} E_{z(i,j,k)}^{n+1} &= E_{z(i,j,k)}^n + \left( \frac{\frac{\Delta t}{\epsilon_o}}{1 + \frac{C\Delta z}{\epsilon_o \Delta x \Delta y}} \right) \nabla \times H_{z(i,j,k)}^{n+\frac{1}{2}} \\ &= E_{z(i,j,k)}^n + \frac{\Delta t}{\epsilon_o \left( 1 + \frac{C\Delta z}{\epsilon_o \Delta x \Delta y} \right)} \nabla \times H_{z(i,j,k)}^{n+\frac{1}{2}} \end{aligned} \quad (6.3.3a)$$

Comparing (6.3.3a) with Canonical FDTD Form:

$$J_{z(i,j,k)}^{n+\frac{1}{2}} = 0 \quad \text{and} \quad \varepsilon_{z(i,j,k)} = \varepsilon_o \left( 1 + \frac{C\Delta z}{\varepsilon_o \Delta x \Delta y} \right) \quad (6.3.3b)$$

From (6.3.3b) the effective permittivity is always positive and the elemental dissipation is zero. The capacitor formulation is therefore proper.

### Linear Dielectric with Loss

For the  $E_z$  field of a linear dielectric with conductivity  $\sigma$ , according to (3.3.4f):

$$\begin{aligned} E_{z(i,j,k)}^{n+1} &= \left( \frac{1-\frac{\sigma\Delta t}{2\varepsilon}}{1+\frac{\sigma\Delta t}{2\varepsilon}} \right) E_{z(i,j,k)}^n + \left( \frac{\frac{\Delta t}{\varepsilon}}{1+\frac{\sigma\Delta t}{2\varepsilon}} \right) \nabla \times H_{z(i,j,k)}^{n+\frac{1}{2}} \\ &= E_{z(i,j,k)}^n + \frac{\Delta t}{\varepsilon \left( 1 + \frac{\sigma\Delta t}{2\varepsilon} \right)} \nabla \times H_{z(i,j,k)}^{n+\frac{1}{2}} - 2 \left( \frac{\frac{\sigma\Delta t}{2\varepsilon}}{1+\frac{\sigma\Delta t}{2\varepsilon}} \right) E_{z(i,j,k)}^n \end{aligned} \quad (6.3.4a)$$

Comparing (6.3.4a) with Canonical FDTD Form:

$$\varepsilon_{z(i,j,k)} = \varepsilon \left( 1 + \frac{\sigma\Delta t}{2\varepsilon} \right) \quad (6.3.4b)$$

$$\frac{\Delta t}{\varepsilon \left( 1 + \frac{\sigma\Delta t}{2\varepsilon} \right)} J_{z(i,j,k)}^{n+\frac{1}{2}} = 2 \left( \frac{\frac{\sigma\Delta t}{2\varepsilon}}{1+\frac{\sigma\Delta t}{2\varepsilon}} \right) E_{z(i,j,k)}^n \quad \Rightarrow \quad J_{z(i,j,k)}^{n+\frac{1}{2}} = \sigma E_{z(i,j,k)}^n \quad (6.3.4c)$$

From (6.3.4b),  $\varepsilon_{z(i,j,k)}$  is always positive, but not the elemental dissipation. Using

$x = E_{z(i,j,k)}^n$ ,  $d = \frac{\sigma\Delta t}{2\varepsilon}$  and  $y = \nabla \times H_{z(i,j,k)}^{n+\frac{1}{2}}$ , the elemental dissipation is:

$$\frac{1}{2} \left( E_{z(i,j,k)}^{n+1} + E_{z(i,j,k)}^n \right) J_{z(i,j,k)}^{n+\frac{1}{2}} = \frac{1}{2} \left[ \frac{1-d}{1+d} x + \frac{\Delta t}{\varepsilon(1+d)} y + x \right] (\sigma x) = \frac{\sigma}{2(1+d)} \left( 2x + \frac{\Delta t}{\varepsilon} y \right) x \quad (6.3.5)$$

This expression is not positive definite, certain combinations of  $x$  and  $y$  will cause it to become negative. To ensure that it is always positive or zero, extra conditions need to be introduced. Requiring that  $\frac{\sigma}{2(1+d)} \left( 2x + \frac{\Delta t}{\varepsilon} y \right) x \geq 0$ :

$$\text{For } x \geq 0: \quad y \geq -\frac{2\varepsilon}{\Delta t} x \Rightarrow \nabla \times H_{z(i,j,k)}^{n+\frac{1}{2}} \geq -2 \frac{\varepsilon}{\Delta t} E_{z(i,j,k)}^n \quad (6.3.6a)$$

$$\text{For } x < 0: \quad y < -\frac{2\varepsilon}{\Delta t} x \Rightarrow \nabla \times H_{z(i,j,k)}^{n+\frac{1}{2}} < -2 \frac{\varepsilon}{\Delta t} E_{z(i,j,k)}^n \quad (6.3.6b)$$

Most of the time the conditions of (6.3.6a) or (6.3.6b) are met, especially when  $\sigma$  is small (low loss at  $\sigma < 10$ ). Extensive real-time examinations of elemental

dissipation during FDTD simulation show that the value is always positive for low to medium loss. Usually the conditions (6.3.6a) and (6.3.6b) do not have to be explicitly imposed during simulation. Equation (6.3.6a) and (6.3.6b) imply that current flowing through the element is always limited. This is similar to an electrical circuit with a few paths having low resistance. Even though the low resistance path can support large current, the circuit configuration will tend to limit the current through the paths, ensuring positive power dissipation. In the case of FDTD simulation, the system model will usually limit the magnetic field components surrounding the electric field so that power dissipation is positive. However since finite-difference is only an approximation to the actual Maxwell's equations, it is expected that the elemental dissipation can become negative once in a while. Extensive simulations show that when  $\sigma$  is substantially greater than 10, the elemental dissipation of (6.3.5) results in negative values once in a while. Most lossy dielectric material will have  $\sigma$  much smaller than 1. When the elemental dissipation is negative, the following equality can be imposed (complying with (6.3.6a) and (6.3.6b) to force  $y = -\frac{2\epsilon}{\Delta t} x$ ):

$$\nabla \times H_{z(i,j,k)}^{n+\frac{1}{2}} = -2\frac{\epsilon}{\Delta t} E_{z(i,j,k)}^n \quad (6.3.7a)$$

Applying (6.3.7a) to the update equation of (6.3.4a) would result in:

$$E_{z(i,j,k)}^{n+1} = -E_{z(i,j,k)}^n \quad (6.3.7b)$$

It is found that using (6.3.7b) for the case when elemental dissipation is negative does not cause any noticeable change in the FDTD simulation results. A typical flow of updating the E field for lossy dielectric with elemental dissipation checking and correction is shown in Figure 6.2. Therefore by modifying the update routine for linear dielectric with loss according to the flow of Figure 6.2, we could again conclude that the formulation is proper. A similar procedure can be used to show that exponential time-stepping scheme (Taflove 1995) for high loss material is also proper, the details are omitted due to lack of space. Formulation such as this where we limit  $\nabla \times H_{z(i,j,k)}^{n+\frac{1}{2}}$  given  $E_{z(i,j,k)}^n$  will be known as conditionally proper.

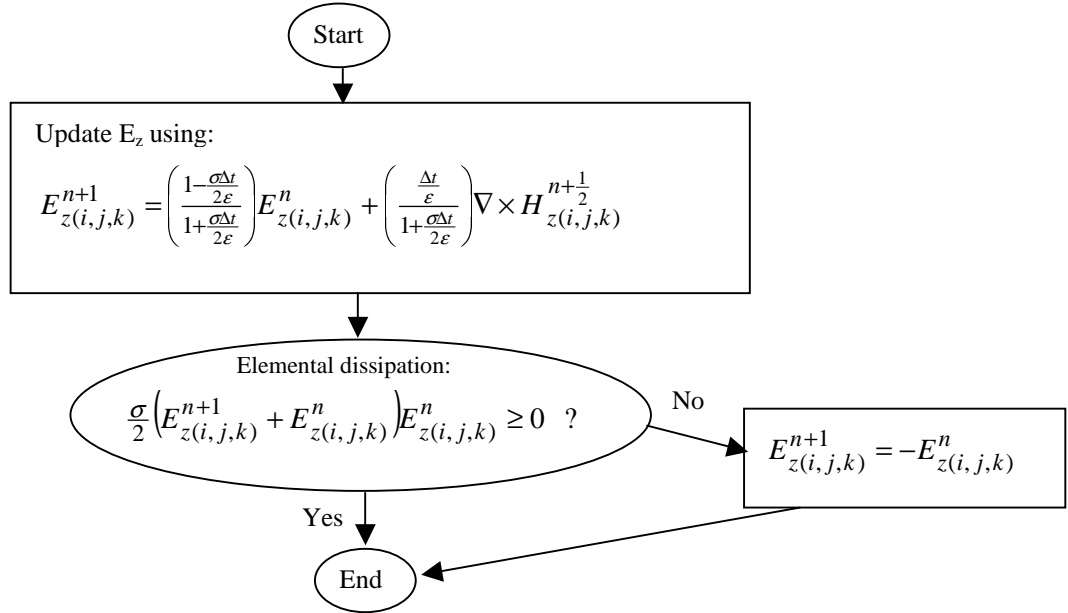


**Figure 6.2** - Modified update routine for linear dielectric with nonzero conductivity.

### Resistor

The update equation for a lumped resistive element of resistance  $R$  is very similar to the form for linear dielectric with loss. We just replace the term  $\sigma$  with  $\frac{\Delta z}{R\Delta x\Delta y}$  in (4.3.4).

$$E_{z(i,j,k)}^{n+1} = \left( \frac{1 - \frac{\Delta t \Delta z}{2\epsilon_0 R \Delta x \Delta y}}{1 + \frac{\Delta t \Delta z}{2\epsilon_0 R \Delta x \Delta y}} \right) E_{z(i,j,k)}^n + \left( \frac{\frac{\Delta t}{\epsilon_0}}{1 + \frac{\Delta t \Delta z}{2\epsilon_0 R \Delta x \Delta y}} \right) \nabla \times H_{z(i,j,k)}^{n+\frac{1}{2}} \quad (6.3.8)$$

Using similar modified update routine as in Figure 6.2, the formulation for resistor is also proper. Again simulation evidence shows that this is not required most of the time, except for low resistance.

### Diode or PN Junction

Consider a PN junction in parallel to the  $z$ -axis, with the update equation for the corresponding electric field given by (using the first order approximation) (4.4.8b):

$$E_{z(i,j,k)}^{n+1} = E_{z(i,j,k)}^n - \frac{C_1}{B_1} \quad (6.3.9)$$

$$C_1 = \frac{N\Delta t}{\epsilon_o \Delta x \Delta y} I_D^n - \frac{\Delta t}{\epsilon_o} \nabla \times H_{z(i,j,k)}^{n+\frac{1}{2}}, \quad B_1 = \frac{\Delta t \Delta z}{\epsilon_o \Delta x \Delta y} \left( \frac{1}{2} \frac{dI_D}{dV} (V^n) + \frac{1}{\Delta t} C^n \right) + 1$$

$$I_D^n = I_s \left( \exp\left(\frac{V^n}{\eta V_T}\right) - 1 \right), \quad V^n = NE_{z(i,j,k)}^n \Delta z, \quad V_T = \frac{kT}{q}$$

$N$  is the orientation constant, it is +1 if the element is oriented in +z direction (i.e. positive current flows in +z direction) as explained in Section 4.4. Let

$$C_2 = \frac{N\Delta t}{\epsilon_o \Delta x \Delta y} I_D^n, \quad (6.3.9) \text{ can be written as:}$$

$$E_{z(i,j,k)}^{n+1} = E_{z(i,j,k)}^n + \frac{\Delta t}{\epsilon_o B_1} \nabla \times H_{z(i,j,k)}^{n+\frac{1}{2}} - \frac{C_2}{B_1}$$

Comparing this with the Canonical FDTD Form:

$$\epsilon_{z(i,j,k)} = \epsilon_o B_1 = \frac{\Delta t \Delta z}{\Delta x \Delta y} \left( \frac{1}{2} \frac{dI_D}{dV} (V^n) + \frac{1}{\Delta t} C^n \right) + \epsilon_o$$

$$\Rightarrow \epsilon_{z(i,j,k)} (E_{z(i,j,k)}^n) = \frac{\Delta t \Delta z}{\Delta x \Delta y} \left( \frac{I_s}{2\eta V_T} \exp\left(\frac{NE_{z(i,j,k)}^n \Delta z}{\eta V_T}\right) + \frac{1}{\Delta t} C^n \right) + \epsilon_o \quad (6.3.10a)$$

$$\frac{\Delta t}{\epsilon_o B_1} J_{z(i,j,k)}^{n+\frac{1}{2}} = \frac{C_2}{B_1} \Rightarrow J_{z(i,j,k)}^{n+\frac{1}{2}} = \frac{\epsilon_o}{\Delta t} C_2 \quad (6.3.10b)$$

From (6.3.10a) the effective permittivity  $\epsilon_{z(i,j,k)}$  is a function of  $E_{z(i,j,k)}^n$  and it is always positive, since  $C^n$  (the junction capacitance) and the exponential term always gives positive values. Let us form the following product to examine the sign of elemental dissipation:

$$D = \frac{1}{2} (E_{z(i,j,k)}^{n+1} + E_{z(i,j,k)}^n) J_{z(i,j,k)}^{n+\frac{1}{2}} = \frac{\epsilon_o}{2\Delta t} \left( 2E_{z(i,j,k)}^n - \frac{C_1}{B_1} \right) C_2 \quad (6.3.11)$$

$D$  is a function of  $E_{z(i,j,k)}^n$  and  $\nabla \times H_{z(i,j,k)}^{n+\frac{1}{2}}$ . Using  $x = E_{z(i,j,k)}^n$  and  $y = \nabla \times H_{z(i,j,k)}^{n+\frac{1}{2}}$ , a plot of  $D(x,y)$  versus  $x$  and  $y$  for a typical surface-mount Schottky diode HSMS-2820 (Agilent Technologies 2000) is shown in Figure 6.3. The diode is oriented in -z direction ( $N = -1$ ) and the range of  $x$  and  $y$  are:

$$x \in [-1000, 7500] \quad , \quad y \in [-5000, 5000]$$

Using  $V = NE_{z(i,j,k)}^n \Delta z$ , the range for  $x$  corresponds to 0.55 to  $-4.125$  Volts, from hard forward biased to hard reverse biased. This range of  $x$  and  $y$  is typically encountered in simulation for low voltage RF circuits. The range could be enlarged to increase the coverage if wished, with similar result obtained. It is seen from Figure 6.3 that  $D$  is weakly influenced by  $y$ . Figure 6.3 confirms that the elemental dissipation is always positive or 0 for normal values of E field. In general it can be shown that this is also true for all practical diode models. Thus from the above arguments, the diode or PN junction formulation is also proper.

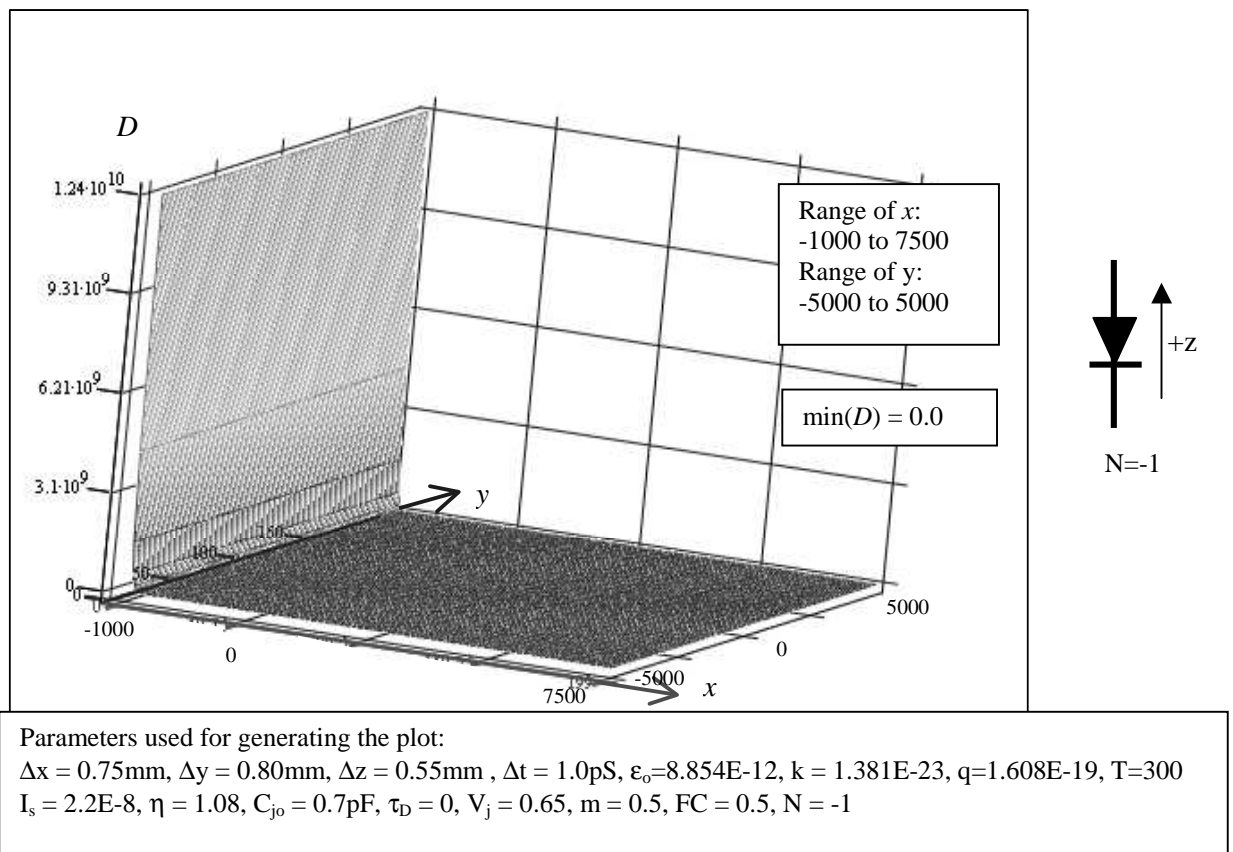


**Figure 6.3** –  $D$  versus  $x = E_{z(i,j,k)}^n$  and  $y = \nabla \times H_{z(i,j,k)}^{n+\frac{1}{2}}$ .

### Bipolar Junction Transistor (BJT)

A procedure similar to analyzing the characteristics of the PN junction can be employed to analyze the BJT. The BJT is formulated according to Section 4.4 where it consists of two PN junctions, the emitter (BE) and the collector (BC) junctions. The elemental dissipation of BE and BC junctions are summed up simultaneously to give the total elemental dissipation of the device. The individual dissipation can be negative, but the total elemental dissipation is always positive or zero as long as the transistor is suitably biased. Assuming the BE and BC junctions are oriented along x-axis as shown in Figure 6.4. It can be shown that when the BJT is not pushed to extreme saturation or cut-off, the BJT formulation is also conditionally proper. This is done by verifying the total device dissipation,  $\varepsilon_{x(i_c, j_c, k_c)}$  and  $\varepsilon_{x(i_e, j_e, k_e)}$  (effective permittivity of BC, BE junctions) are positive definite within the four operating regions of a BJT, i.e. active, saturation, inverse and cut-off regions. The BJT formulation is thus conditionally proper. From Section 4.4:

$$E_{x(i_c, j_c, k_c)}^{n+1} = E_{x(i_c, j_c, k_c)}^n + \frac{C_1 E_2 - C_2 E_1}{B_2 E_1 - B_1 E_2} \quad (6.3.12a)$$

$$E_{x(i_e, j_e, k_e)}^{n+1} = E_{x(i_e, j_e, k_e)}^n + \frac{B_1 C_2 - B_2 C_1}{B_2 E_1 - B_1 E_2} \quad (6.3.12b)$$

Define new variables  $C_1'$  and  $\Delta$ :

$$C_1' = \frac{\Delta t N_c}{\varepsilon \Delta y \Delta z} I_{CS}^n \quad (6.3.13a)$$

$$\Delta = B_1 E_2 - B_2 E_1 \quad (6.3.13b)$$

From (4.4.15c),  $C_1$  can be written as:

$$C_1 = \frac{\Delta t N_c}{\varepsilon \Delta y \Delta z} I_{CS}^n - \frac{\Delta t}{\varepsilon} \left( \nabla \times \vec{H}_{C(i_c, j_c, k_c)}^{n+\frac{1}{2}} \right) = C_1' - \frac{\Delta t}{\varepsilon} \left( \nabla \times \vec{H}_{C(i_c, j_c, k_c)}^{n+\frac{1}{2}} \right) \quad (6.3.14)$$

Substituting this into (6.3.12a):

$$E_{x(i_c, j_c, k_c)}^{n+1} = E_{x(i_c, j_c, k_c)}^n + \frac{\Delta t}{\varepsilon \left( \frac{\Delta}{E_2} \right)} \nabla \times \vec{H}_{C(i_c, j_c, k_c)}^{n+\frac{1}{2}} - \left( -\frac{C_2 E_1 - C_1' E_2}{\Delta} \right) \quad (6.3.15)$$

Compare (6.3.15) with the Canonical FDTD Update Form. The following expressions will be obtained.

$$\mathcal{E}_{x(i_c, j_c, k_c)} = \mathcal{E} \frac{\Delta}{E_2} \quad (6.3.16a)$$

$$J_{x(i_c, j_c, k_c)}^{n+\frac{1}{2}} = \frac{\mathcal{E}}{\Delta t} \cdot \frac{C_1' E_2 - C_2 E_1}{E_2} \quad (6.3.16b)$$

Following similar procedures, (6.3.12b) can be written as:

$$E_{x(i_e, j_e, k_e)}^{n+1} = E_{x(i_e, j_e, k_e)}^n + \frac{\Delta t}{\mathcal{E} \left( \frac{\Delta}{B_1} \right)} \nabla \times \vec{H}_{E(i_e, j_e, k_e)}^{n+\frac{1}{2}} - \left( -\frac{B_2 C_1 - C_2 B_1}{\Delta} \right) \quad (6.3.17a)$$

$$C_2' = \frac{\Delta t N_E}{\mathcal{E} \Delta y \Delta z} I_{ES}^n \quad (6.3.17b)$$

$$\mathcal{E}_{x(i_e, j_e, k_e)} = \mathcal{E} \frac{\Delta}{B_1} \quad (6.3.17c)$$

$$J_{x(i_e, j_e, k_e)}^{n+\frac{1}{2}} = \frac{\mathcal{E}}{\Delta t} \cdot \frac{C_2 B_1 - C_1 B_2}{B_1} \quad (6.3.17d)$$

As in the PN junction formulation, the characteristics of an actual NPN transistor is tested. The transistors used are BFR92A and BFG520 from Phillips Semiconductor (Phillips Semiconductor, 1995 and 1997). BFR92A is a wideband NPN transistor with transition frequency  $f_T$  (Gray and Meyer, 1993) up to 5.0GHz. BFG520 is an ultra-wideband NPN transistor with  $f_T = 9.0$ GHz. The orientation of BE and BC junctions for both transistors is assumed as shown in Figure 6.4, which amount to  $N_E = -1$ ,  $N_C = 1$ .

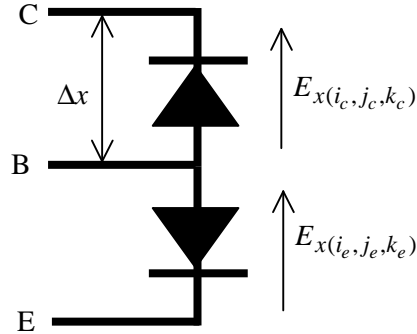


**Figure 6.4** – Orientation of BE and BC junctions for transistor BFR92A and BFG520.

Begin by verifying that the total device dissipation is positive definite within suitable operating conditions. Then show that within these suitable conditions,  $\varepsilon_{z(i_c, j_c, k_c)}$  and  $\varepsilon_{z(i_e, j_e, k_e)}$  are always positive. First define the total device dissipation as:

$$D = \frac{1}{2} \left[ \left( E_{z(i_c, j_c, k_c)}^{n+1} + E_{z(i_c, j_c, k_c)}^n \right) J_{z(i_c, j_c, k_c)}^{n+\frac{1}{2}} + \left[ \left( E_{z(i_e, j_e, k_e)}^{n+1} + E_{z(i_e, j_e, k_e)}^n \right) J_{z(i_e, j_e, k_e)}^{n+\frac{1}{2}} \right] \right]$$

This can be rewritten in a more compact form as:

$$D = D(x_e, x_c, y_e, y_c) \quad (6.3.18)$$

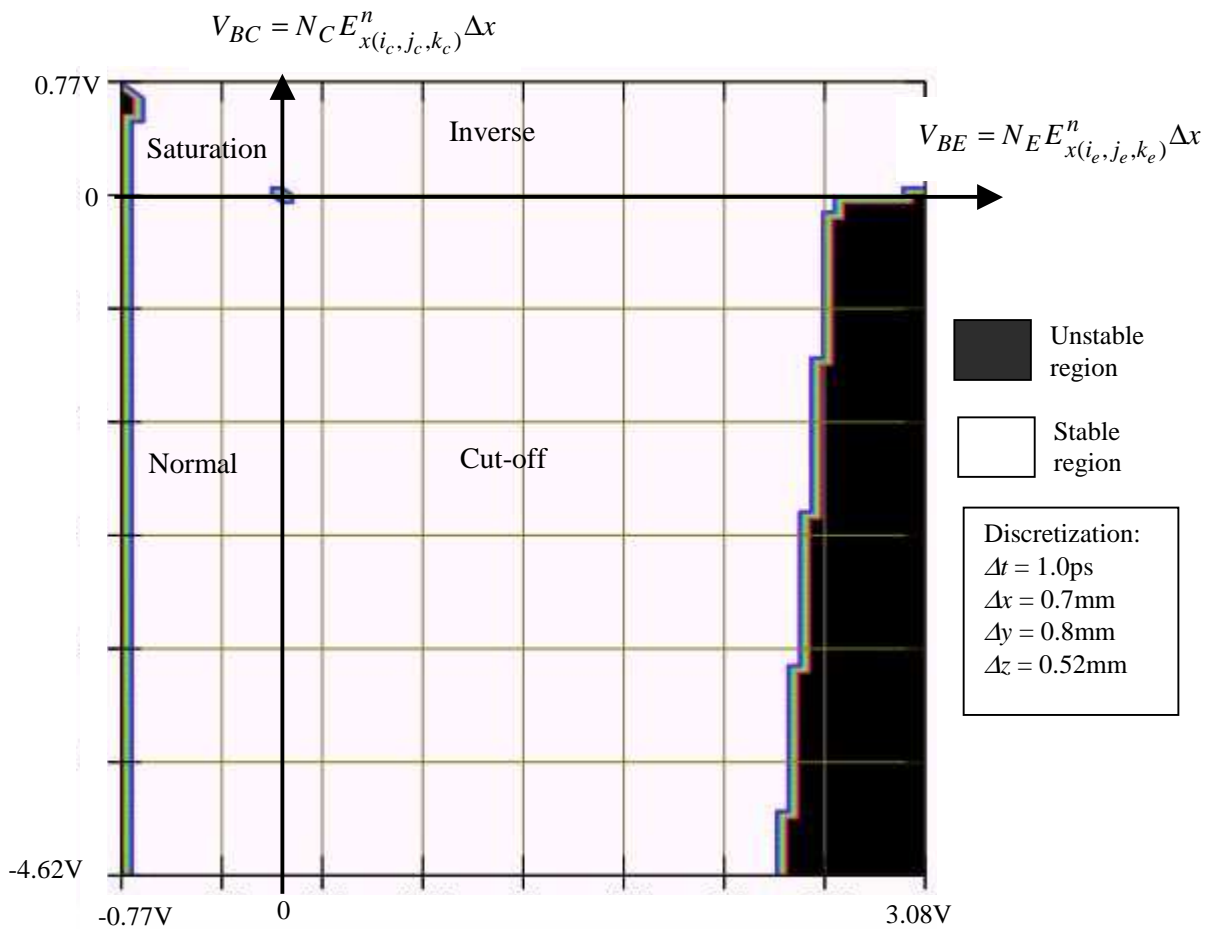
where  $x_e = E_{x(i_e, j_e, k_e)}^n$ ,  $x_c = E_{x(i_c, j_c, k_c)}^n$ ,  $y_e = \nabla \times \vec{H}_{E(i_e, j_e, k_e)}^{n+\frac{1}{2}}$  and  $y_c = \nabla \times \vec{H}_{C(i_c, j_c, k_c)}^{n+\frac{1}{2}}$ .

It is impossible to plot  $D$  as a function of these variables as fifth dimensional space is required. Instead an exhaustive search is carried out using a computer, by calculating the value of  $D$  within a domain  $G$  as follows for transistor BFR92A and BFG520:

$$G_{BFR92A} = \left\{ (x_e, x_c, y_e, y_c) : \begin{array}{l} x_e \in [-1400, 5600], x_c \in [-8400, 1400], \\ y_e \in [-2000, 2000], y_c \in [-2000, 2000] \end{array} \right\} \quad (6.3.19a)$$

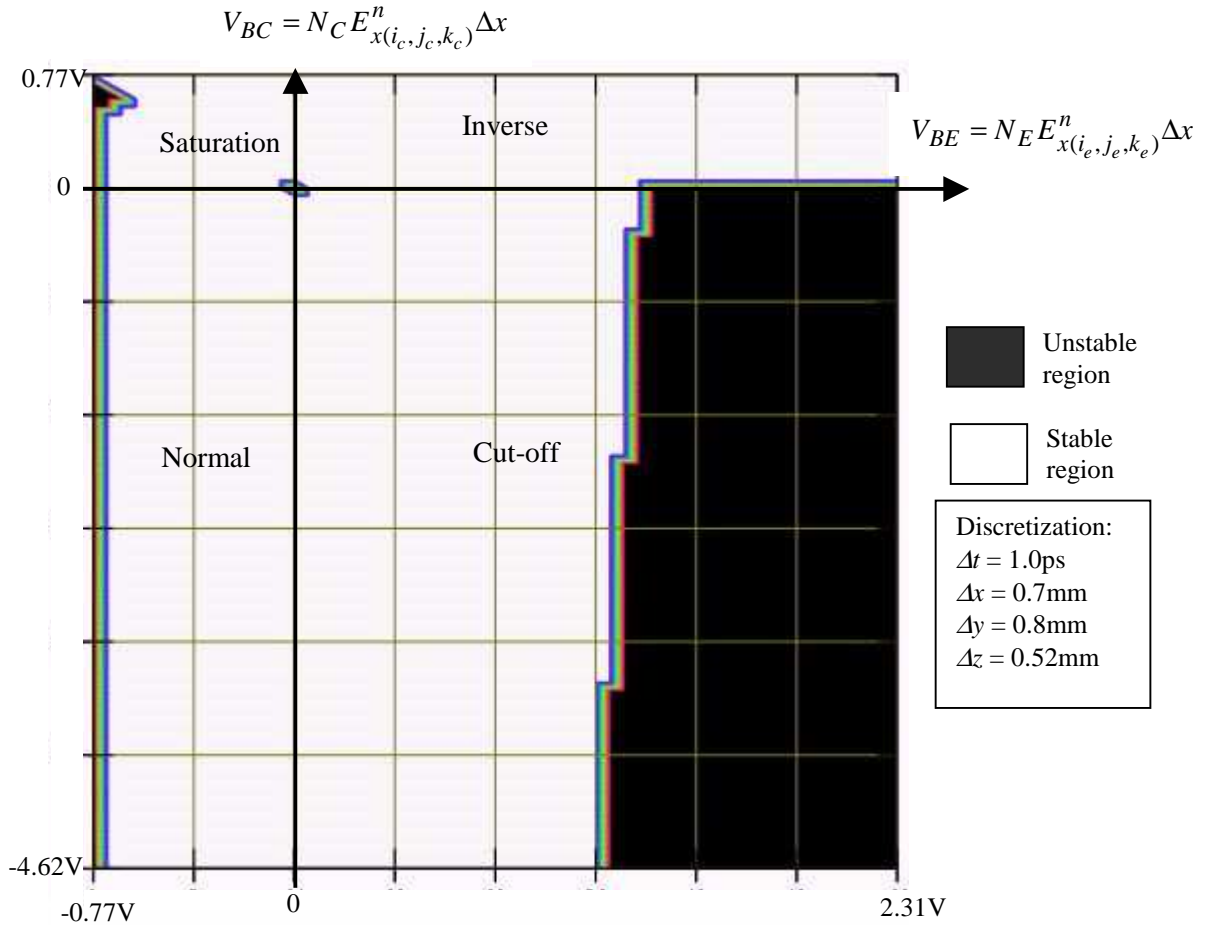
$$G_{BFG520} = \left\{ (x_e, x_c, y_e, y_c) : \begin{array}{l} x_e \in [-1400, 4200], x_c \in [-8400, 1400], \\ y_e \in [-2000, 2000], y_c \in [-2000, 2000] \end{array} \right\} \quad (6.3.19b)$$

The search is carried out in discrete steps with  $\Delta x_e = 20$ ,  $\Delta x_c = 20$ ,  $\Delta y_e = 20$ ,  $\Delta y_c = 20$ . This domain encompasses the four operating regions of a BJT for various values of collector and emitter current. The limits for  $x_e$  and  $x_c$  allow BE and BC junctions to undergo hard forward-biased and hard reverse-biased. The limits for  $y_e$  and  $y_c$  are those typically encountered in the simulation of low power RF circuits. For both transistors it is observed that  $D$  is weakly influenced by  $y_e$  and  $y_c$ . Allowing for  $-2000 \leq y_e, y_c \leq 2000$ , the regions for  $x_e$  and  $x_c$  where  $D$  is positive is called the BJT stable region. This is shown in Figure 6.5a and Figure 6.5b for BFR92A and BFG520 respectively. The dark region corresponds to unstable region of the transistors, while the light region is the stable region with  $-2000 \leq y_e, y_c \leq 2000$ .



**Gummel-Poon Model for BFR92A**  
 $I_{ss}=4.1188E-16$  ,  $\beta_F=102.64$  ,  $\beta_R=18.11$  ,  $n_F=0.99728$  ,  $n_R=0.99620$  ,  $V_A=62.672$  ,  $I_{KF}=3.201$  ,  
 $I_{SE}=4.0106E-15$  ,  $n_E=1.5771$  ,  $V_B=3.3692$  ,  $I_{KR}=1.28155$  ,  $I_{SC}=2.7991E-16$  ,  $n_C=1.0754$  ,  $V_{JE}=0.60$  ,  
 $m_E=0.25857$  ,  $C_{JE}=8.9051E-13$  ,  $\tau_F=1.5497E-11$  ,  $V_{JC}=0.38082$  ,  $m_C=0.20294$  ,  $C_{JC}=5.4656E-13$  ,  
 $\tau_R=0$  ,  $FC=0.5$  ,  $r_B=10$  ,  $N_C = 1$  ,  $N_E = -1$ .

**Figure 6.5a** – Plot of  $D$  versus  $x_e$  and  $x_c$  for  $-2000 \leq y_e, y_c \leq 2000$  (BFR92A).



**Gummel-Poon Model for BFG520**

$I_{ss}=1.0168E-15$  ,  $\beta_F=220.182$  ,  $\beta_R=100.714$  ,  $n_F=1.00065$  ,  $n_R=0.99811$  ,  $V_A=48.062$  ,  $I_{KF}=0.51004$  ,  
 $I_{SE}=2.83095E-13$  ,  $n_E=2.03568$  ,  $V_B=1.6929$  ,  $I_{KR}=2.3526E-03$  ,  $I_{SC}=2.44898E-17$  ,  $n_C=1.02256$  ,  
 $V_{JE}=0.60$  ,  $m_E=0.258153$  ,  $C_{JE}=1.24548E-12$  ,  $\tau_F=8.61625E-12$  ,  $V_{JC}=0.189234$  ,  $m_C=0.3333$  ,  
 $C_{JC}=4.47646E-13$  ,  $\tau_R=0$  ,  $FC=0.5$  ,  $r_B=10$  ,  $N_C = 1$  ,  $N_E = -1$ .

**Figure 6.5b** – Plot of  $D$  versus  $x_e$  and  $x_c$  for  $-2000 \leq y_e, y_c \leq 2000$  (BFG520).

From both Figure 6.5a and Figure 6.5b, it is observed that the BJT model according to Section 4.4 will have negative device dissipation when the BE junction of the transistor is heavily forward-biased and heavily reverse-biased. Therefore the BJT formulation is conditionally stable. As long as during the simulation we can prevent the operating point of the BJT from drifting into the darken regions of Figure 6.5a and Figure 6.5b, the BJT devices BFR92A and BFG520 will be stable. There is a small region in the vicinity of  $(x_e, x_c) = (0, 0)$  where the device dissipation is negative for both

BFR92A and BFG520. Upon closer scrutiny of this region by using exhaustive search, the minimum value of  $D$  in this region is very small, for BFR92A it occurs approximately at  $(x_e, x_c, y_e, y_c) = (0, 0, -1000, 1500)$  with  $D(0, 0, -1000, 1500) = -1.42259 \times 10^{-11}$ . For BFG520, this occurs approximately at  $(x_e, x_c, y_e, y_c) = (0, 0, 0, 1500)$ , with  $D(0, 0, 0, 1500) = -3.09542 \times 10^{-11}$ . Since  $D$  is very small and close to zero its effect is negligible, the BJT operating condition will not linger in this region for long, the moment the BE and BC junction voltage is not zero, the device dissipation will become positive again. The same can be said for BFG520. To further strengthen the confidence that there is indeed no other point in the stable region that results in negative  $D$ , the Method of Steepest Descent (Wismer and Chattergy, 1978) is carried out in a few randomly chosen points in the four operating regions of the BJT. Again this does not yield any point with negative  $D$  in the unshaded regions.

The final step is to verify that both  $\varepsilon_{x(i_c, j_c, k_c)}$  and  $\varepsilon_{x(i_e, j_e, k_e)}$  are positive always.

Expanding (6.3.16a) and (6.3.17c):

$$\varepsilon_{x(i_c, j_c, k_c)} = \varepsilon \frac{\Delta}{E_2} = \varepsilon \left( B_1 - B_2 \frac{E_1}{E_2} \right) \quad (6.3.20a)$$

$$\varepsilon_{x(i_e, j_e, k_e)} = \varepsilon \frac{\Delta}{B_1} = \varepsilon \left( E_2 - E_1 \frac{B_2}{B_1} \right) \quad (6.3.20b)$$

From the definition of  $B_1$ ,  $B_2$ ,  $E_1$  and  $E_2$  in Section 4.4, these variables only depend on  $x_e = E_{x(i_e, j_e, k_e)}^n$  and  $x_c = E_{x(i_c, j_c, k_c)}^n$ . A plot of  $\varepsilon_{x(i_c, j_c, k_c)}$  and  $\varepsilon_{x(i_e, j_e, k_e)}$  versus  $x_e$  and  $x_c$  is shown in Figure 6.6. This confirms that the effective permittivity is always positive in the stable regions of BFR92A and BFG520. The parameters for both transistors are similar to the parameters used in generating Figure 6.5a and Figure 6.5b. Another way to show this statement is to note that:

$$E_2 = \frac{\Delta t \Delta x}{\varepsilon \Delta y \Delta z} \left( \frac{1}{2} \frac{\partial I_{ES}}{\partial V_{BE}} \Big|_{V_{BE}^n} + \frac{C_E^n}{\Delta t} \right) + 1 \quad (6.3.21a)$$

$$B_1 = \frac{\Delta t \Delta x}{\varepsilon \Delta y \Delta z} \left( \frac{1}{2} \frac{\partial I_{CS}}{\partial V_{BC}} \Big|_{V_{BC}^n} + \frac{C_C^n}{\Delta t} \right) + 1 \quad (6.3.21b)$$

The differentiation of the current  $I_{ES}$  and  $I_{CS}$  are nominally positive for proper transistor model (since currents are in exponential form) and the junction capacitance  $C_E$  and  $C_C$  are also always positive. Thus  $E_2$  and  $B_I$  are positive. By plotting  $\Delta$  versus  $x_e$  and  $x_c$ , if  $\Delta$  is always positive in the region of interest, then  $\varepsilon_{x(i_c, j_c, k_c)}$  and  $\varepsilon_{x(i_e, j_e, k_e)}$  will also be positive as these are just  $\varepsilon$  multiplying  $\Delta$  and divided with  $E_2$  and  $B_I$  respectively.

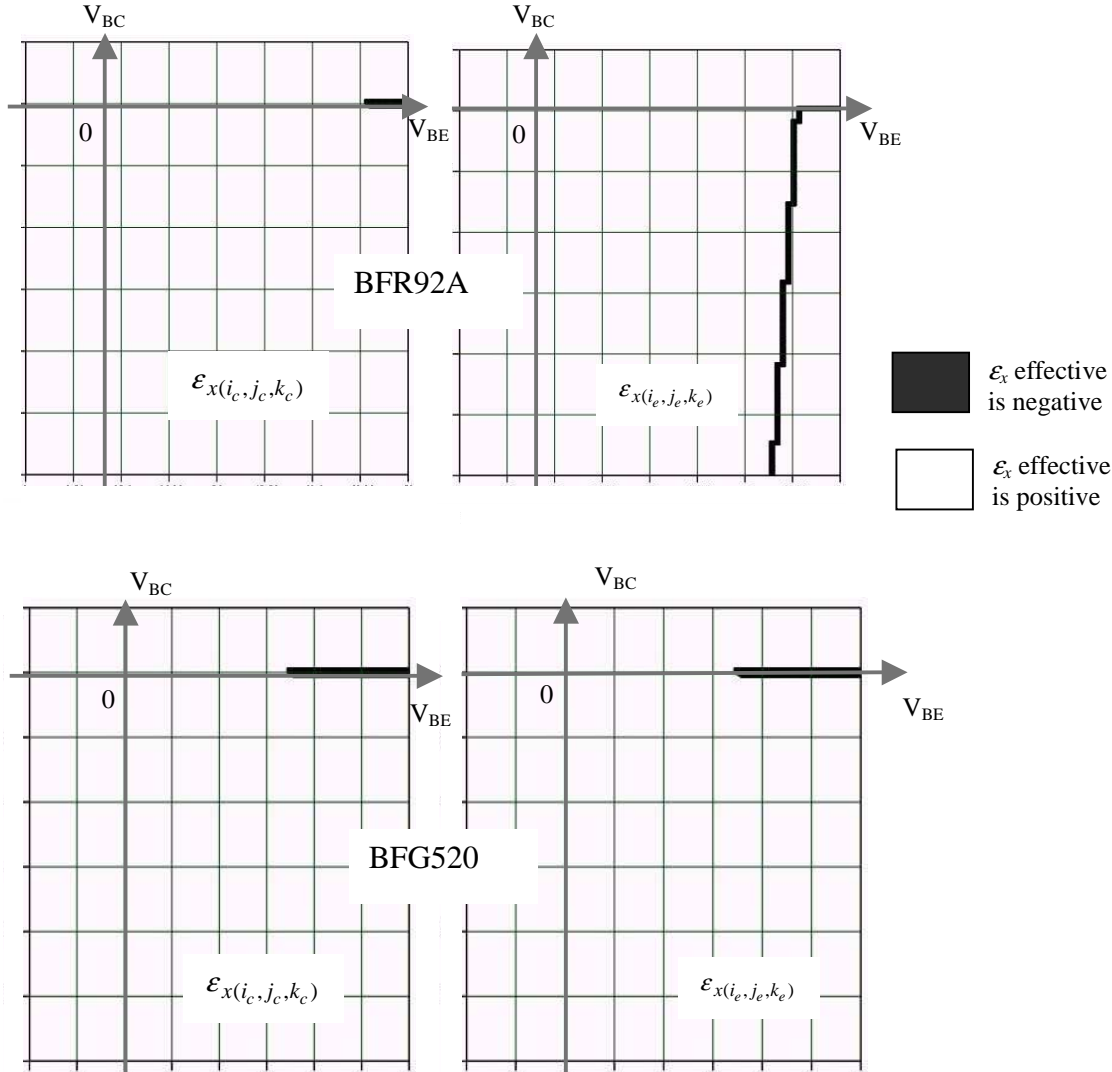


**Figure 6.6** -  $\varepsilon_{x(i_c, j_c, k_c)}$  and  $\varepsilon_{x(i_e, j_e, k_e)}$  versus  $x_e$  and  $x_c$  for BFR92A and BFG520 transistor. The range for  $x_e$  and  $x_c$  is similar to the ranges in Figure 6.5a and Figure 6.5b.

Now suppose the model consists of many cubes of similar size, with  $\Delta x = 0.75\text{mm}$ ,  $\Delta y = 0.8\text{mm}$ ,  $\Delta z = 0.52\text{mm}$ . The model is non-magnetic, but the dielectric constant is not uniform, with variation of  $\epsilon$  across the model and a portion of the model is free space. Also from (6.3.1b), (6.3.3b), (6.3.4b), (6.3.10b), (6.3.20a) and (6.3.20b), the effective permittivity  $\epsilon_{r(i,j,k)}$  is always be greater than  $\epsilon_o$ . From this information, we conclude that the smallest permittivity equals to  $\epsilon_o$  as any dielectric, which is not air, will have  $\epsilon_r$  greater than unity. Using condition (6.2.4b) of Lemma 6.2:

$$c_m = \frac{1}{\sqrt{\mu_o \epsilon_o}} \cong \frac{1}{\sqrt{(4\pi \times 10^{-7})(8.854 \times 10^{-12})}} \cong 2.99796 \times 10^8$$

$$\Delta t < \min \left\{ \begin{array}{l} \left( c_m \sqrt{2} \sqrt{\frac{1}{\Delta y^2} + \frac{1}{\Delta z^2}} \right)^{-1} = 1.02835 \times 10^{-12}, \left( c_m \sqrt{2} \sqrt{\frac{1}{\Delta x^2} + \frac{1}{\Delta z^2}} \right)^{-1} = 1.0079 \times 10^{-12}, \\ \left( c_m \sqrt{2} \sqrt{\frac{1}{\Delta x^2} + \frac{1}{\Delta y^2}} \right)^{-1} = 1.2905 \times 10^{-12} \end{array} \right\}$$

$$\Rightarrow \Delta t < 1.0079 \times 10^{-12}$$

Compare this with CFL Criteria:

$$\Delta t < \frac{1}{c_m \sqrt{\frac{1}{\Delta x^2} + \frac{1}{\Delta y^2} + \frac{1}{\Delta z^2}}} = 1.2573 \times 10^{-12}$$

The new stability criterion has an increase in restriction by 19.84%. Finally it can be concluded that if all elements used have update equations of the above and  $\Delta t < 1.0079 \times 10^{-12}$ , then according to Lemma 6.2 and Theorem 6.3, the model of Figure 6.1 will be stable. This means that if the initial E and H field components at time-step  $n = 0$  is not zero, all field components will remain bounded as we advance the time-step  $n$ .

Notice that throughout this section the only requirement for the effective permittivity  $\epsilon_{r(i,j,k)}$  is that it is positive. Thus the permittivity can change with location, be a nonlinear function of field components and yet the sourceless 3D model is still stable. So the method proposed here could also be used to prove the stability of model with non-homogeneous dielectric and nonlinear dielectric. In the next section, the case when there is a resistive voltage source in the model will be considered.

#### 6.4 Extension of the Stability Theorem to 3D Model with Source

Suppose in addition to the elements mentioned in Section 6.3, the 3D model of Figure 6.1 also contains a lumped resistive voltage source, with update equation for  $E_z$  field given by (4.3.5):

$$E_{z(i,j,k)}^{n+1} = \left( \frac{1-D_z}{1+D_z} \right) E_{z(i,j,k)}^n + \frac{\Delta t}{\varepsilon(1+D_z)} \nabla \times H_{z(i,j,k)}^{n+\frac{1}{2}} - \left[ \frac{2D_z}{(1+D_z)\Delta z} \right] V\left(n + \frac{1}{2}\right) \quad (6.4.1)$$

Where  $D_z = \frac{\Delta t \Delta z}{2R_s \varepsilon \Delta x \Delta y}$ ,  $V\left(n + \frac{1}{2}\right)$  is the independent voltage source as a function of time-step  $n$  and  $R_s$  being the source resistance.  $V\left(n + \frac{1}{2}\right)$  can represent a constant d.c. source, a pulse, sinusoidal function and so forth. Converting (6.4.1) into the Canonical FDTD Form, we observe that the equivalent current density is:

$$J_{z(i,j,k)}^{n+\frac{1}{2}} = \frac{\Delta z}{R_s \Delta x \Delta y} \left( E_{z(i,j,k)}^n + \frac{V\left(n+\frac{1}{2}\right)}{\Delta z} \right) \quad (6.4.2)$$

By introducing  $x = E_{z(i,j,k)}^n$ ,  $y = \nabla \times H_{z(i,j,k)}^{n+\frac{1}{2}}$  and  $v = \frac{V\left(n+\frac{1}{2}\right)}{\Delta z}$ , the elemental dissipation can be written as:

$$\begin{aligned} D^{n+\frac{1}{2}}(x, y, v) &= \frac{1}{2} \left( E_{z(i,j,k)}^{n+1} + E_{z(i,j,k)}^n \right) J_{z(i,j,k)}^{n+\frac{1}{2}} \\ &= \frac{\Delta z}{2R_s \Delta x \Delta y} \cdot \frac{1}{1+D_z} \left[ 2x + \frac{\Delta t}{\varepsilon} y \right] x - \frac{\Delta z}{2R_s \Delta x \Delta y} \cdot \frac{1}{1+D_z} \left[ 2D_z v - \frac{\Delta t}{\varepsilon} y - 2(1-D_z)x \right] v \end{aligned} \quad (6.4.3)$$

Again this equation is indefinite,  $D^{n+\frac{1}{2}}$  can be positive or negative. When source element such as (6.4.1) is present,  $P_d$  can become positive and from Lemma 6.1 the numerical energy  $V^n$  of the model can increase with time-step. Assuming  $v$  is a constant positive value (we can consider it to be a d.c. voltage source), a plot of the region **A** in the  $x$ - $y$  plane where elemental dissipation  $D^{n+\frac{1}{2}}$  becomes negative is shown in Figure 6.7. A similar but inverted region can be easily plotted when  $v$  is a constant negative value.

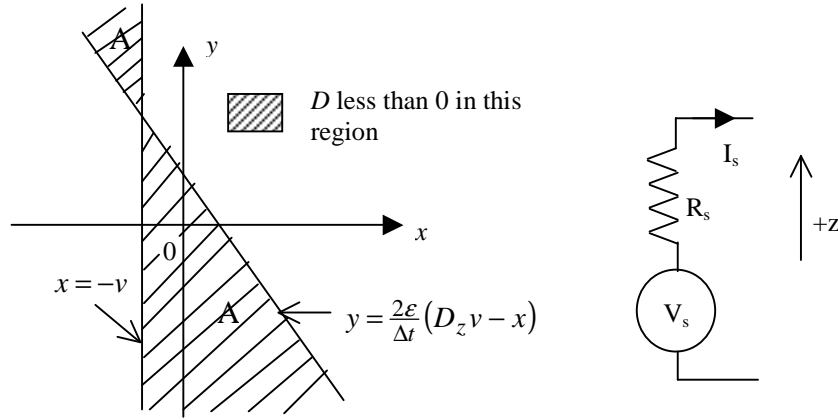


**Figure 6.7** – Negative region **A** of the resistive voltage source when  $v > 0$  and is constant.

A pertinent question is whether there is any further constraint apart from region **A**? In fact there is. The first constraint is the current  $I_s$  (see Figure 6.7) must not be more than  $V_s / R_s$ , which represents the source current when the terminals are shorted. There are cases when source current can exceed this limit but for a properly designed circuit  $V_s / R_s$  is usually the threshold. The second constraint is for the source of (6.4.1) to continuously supply power to the model, elemental dissipation must always be negative or zero at all sequence  $n$ . This means if  $(x,y)$  of sequence  $n$  result in  $D^{n+\frac{1}{2}} \leq 0$ , then  $(x, y)$  of sequence  $n+1$  must also result in  $D^{n+\frac{3}{2}} \leq 0$ . Appendix 5 shows that these requirements can be expressed mathematically as:

$$y < \frac{2\varepsilon}{\Delta t} (D_z v - x) \quad (6.4.4a)$$

$$D^{n+\frac{1}{2}}(x, y, v) \leq 0 \quad (6.4.4b)$$

$$x^{n+1} = \left( \frac{1-D_z}{1+D_z} \right) x^n + \frac{\Delta t}{\varepsilon(1+D_z)} y^{n+\frac{1}{2}} - \frac{2D_z}{1+D_z} v \geq -v \quad (6.4.4c)$$

Using the criteria of (6.4.4a)-(6.4.4c), and assuming  $V(n + \frac{1}{2}) = 1$ , a new negative region, called **B** is shown in Figure 6.8a for  $D_z < 1$  and Figure 6.8b for  $D_z > 1$ . When  $(x,y)$  is outside the shaded region **B**, the resistive voltage source will bound to stop

supplying numerical power to the model in future sequence and the E and H field components will start to decrease.

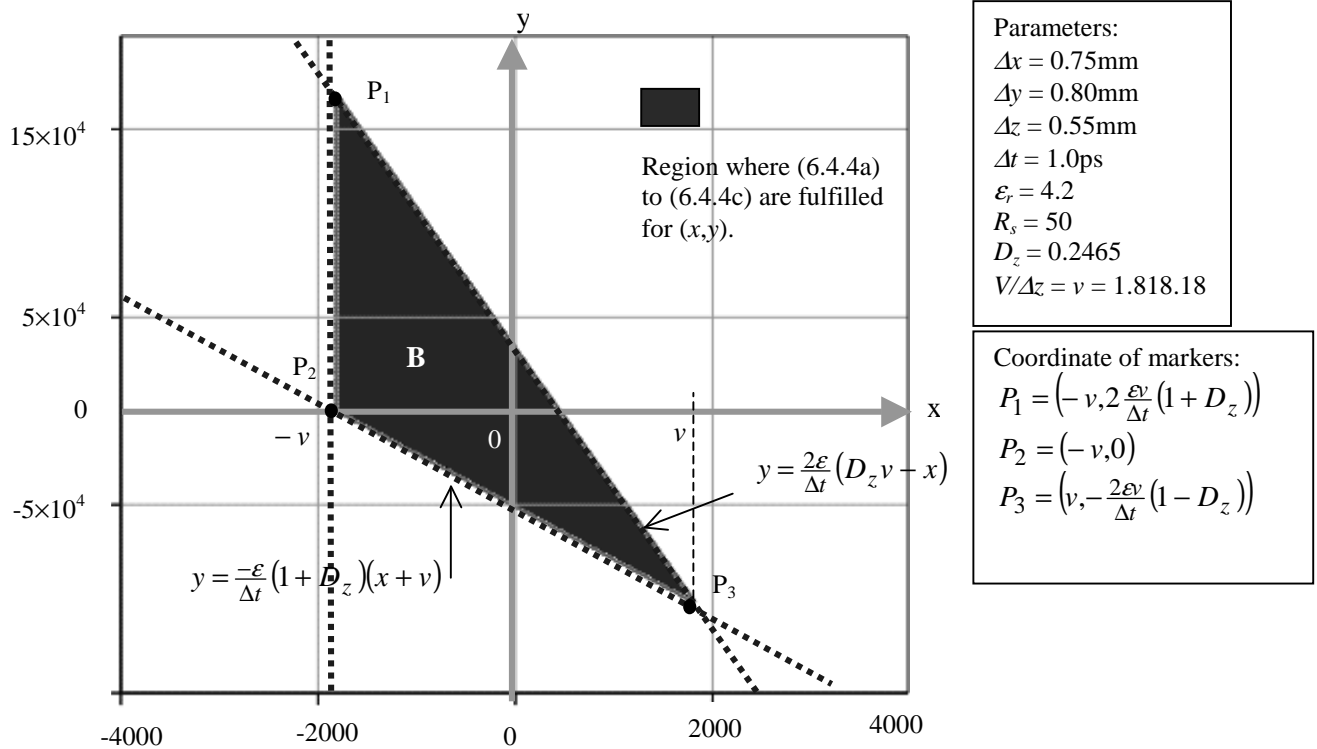


**Figure 6.8a** – Negative region for resistive voltage source fulfilling (6.4.4a) to (6.4.4c),

$D_z < 1$ .  $P_1$  to  $P_3$  are marker points.

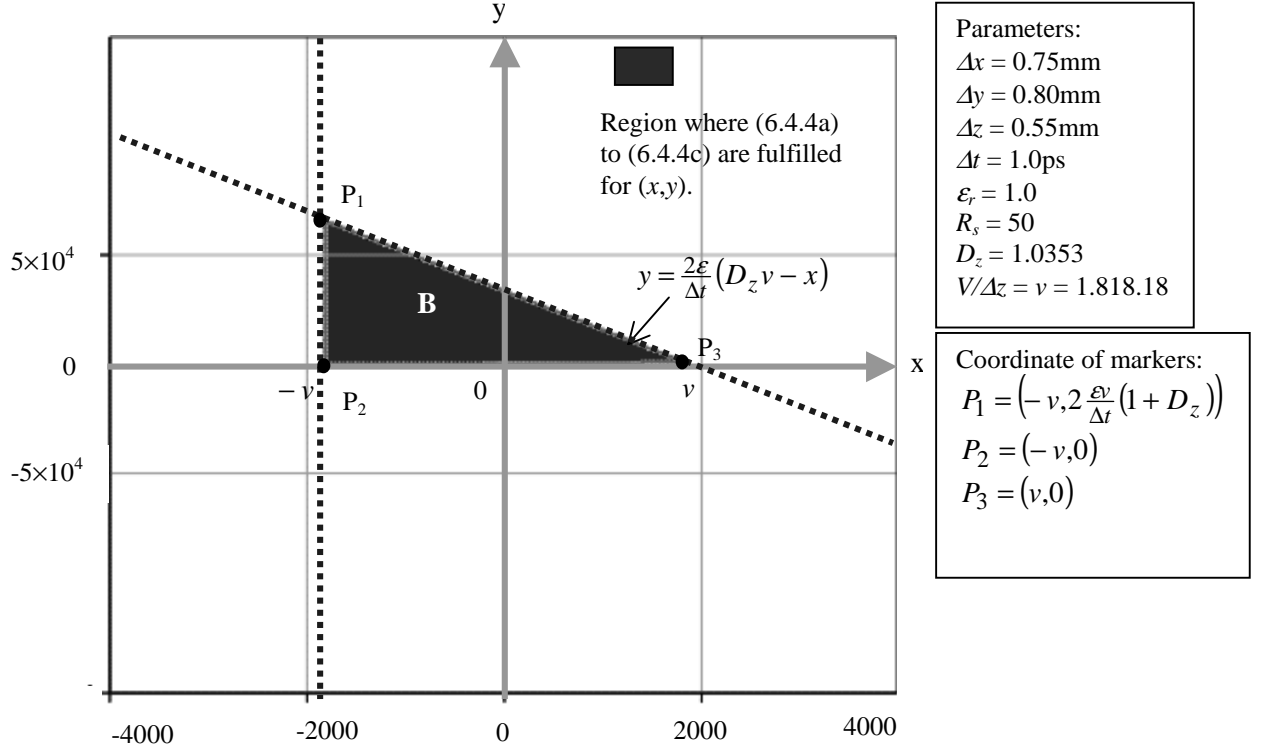


**Figure 6.8b** – Negative region for resistive voltage source fulfilling (6.4.4a) to (6.4.4c),  $D_z > 1$ .

The negative regions **B** identified in Figure 6.8a and Figure 6.8b are still quite conservative, nevertheless it is sufficient for the next argument. In order to have  $D^{n+\frac{1}{2}} \leq 0$  for all  $n$ , the actual region could be smaller than shown. For a resistive voltage source to continuously supply numerical energy to the model, its state  $(x,y)$  must always be confined to **B**. Furthermore if the source  $V(n+\frac{1}{2})$  is not constant, then we can construct the negative region based on the largest magnitude of  $V(n+\frac{1}{2})$ . Negative regions for resistive voltage source when  $V(n+\frac{1}{2})$  is negative can be constructed in a similar manner using (6.4.4a)-(6.4.4c). The importance of the negative regions can be summed up as follows. Suppose an FDTD model as in Figure 6.1

contains all proper or conditionally proper formulations and a few resistive voltage sources. Then initially the numerical energy  $V^n$  of the system will increase. Since in Appendix 4 it has been proven that  $V^n$  is radially unbounded to all field components, a diverging  $V^n$  will entail at least one or more E or H field components that are increasing. Due to the propagating nature of Maxwell's equations, a field component that is increasing without limit will subsequently cause the rest of the model's E and H field components to increase too. The important feature of the negative regions is that it is bounded as long as the source voltage  $V_s$  is bounded and  $R_s$  greater than 0. If the increment of  $V^n$  is not limited by other dissipative elements in the model,  $(x,y)$  will eventually cross the boundary of the negative region. Then the elemental dissipation of the resistive voltage source will bound to become positive again and the increment of numerical energy halts. Thus there is a built-in mechanism (due to  $R_s$ ) in the resistive voltage source formulation to prevent uncontrolled increment of the field components. With this we can conclude that the general FDTD model with resistive voltage sources will be numerically stable if and only if the following three conditions are met:

1. Theorem 6.3 is fulfilled when the model does not contain any source.
2. There is no other source except resistive voltage sources.
3. FDTD formulations of other elements are proper or conditionally proper.

### 6.5 Simulation Example

A simulation is carried out to verify the concepts discussed. Here a short conducting trace energized by a resistive voltage source is connected to a parallel RC load. The PEC boundary is used in this experiment. The schematic and the top view of the FDTD model is shown in Figure 6.9. The simulated voltage across the resistive voltage source and the load is shown in Figure 6.10(A), while the numerical energy  $V^n$  is shown in Figure 6.10(B). In this model the resistive voltage source is immersed in the dielectric and is z directed. Its voltage function is a single pulse of amplitude 3.3V, active during 0 – 2100ps and then set to 0 beyond 2100ps. As seen in Figure 6.10(B) when the voltage source is active,  $V^n$  increases rapidly and then saturates, as the 'power' supplied by the source equals the 'power' dissipated by the resistors in the model. During active

stage the state  $(x,y)$  of the resistive voltage source is determined from the corresponding E and H fields and plotted in the x-y plane of Figure 6.11. From the result we could clearly see that the coordinate never leaves the negative region. After the voltage  $V_s$  is deactivated, the resistive voltage source reverts to a normal resistor model. We observe that the numerical energy  $V^n$  of the model starts to decline, as now all the elements in the model are proper.

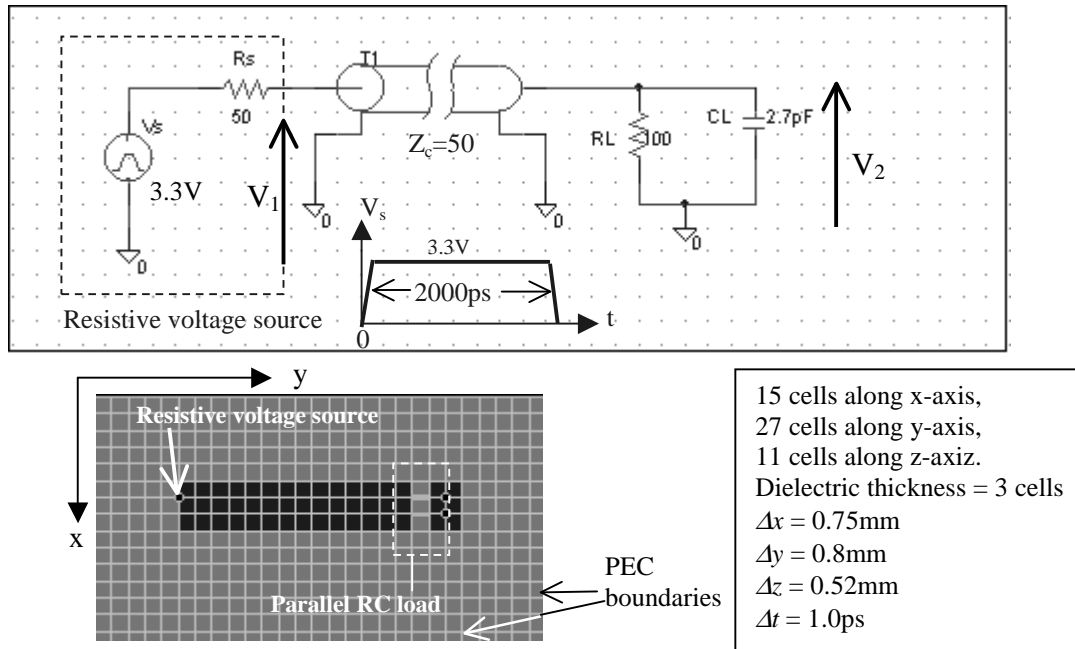


**Figure 6.9** – The schematic and top view of the test model.

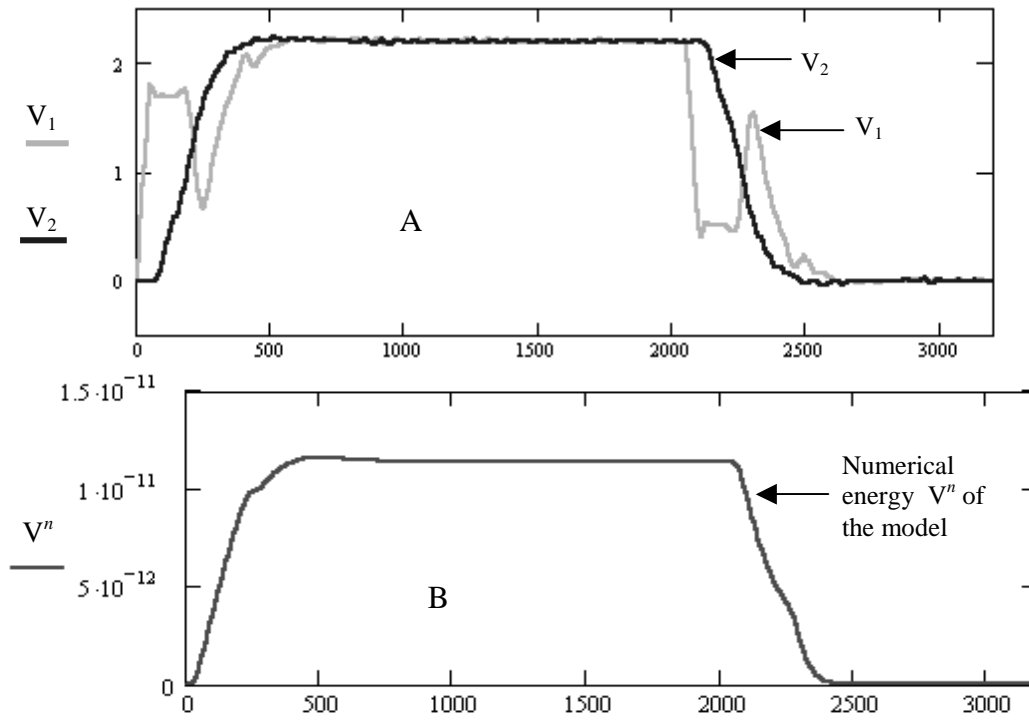


**Figure 6.10** – (A) Voltage across the resistive voltage source and the RC load. (B) Numerical energy  $V''$  of the system.

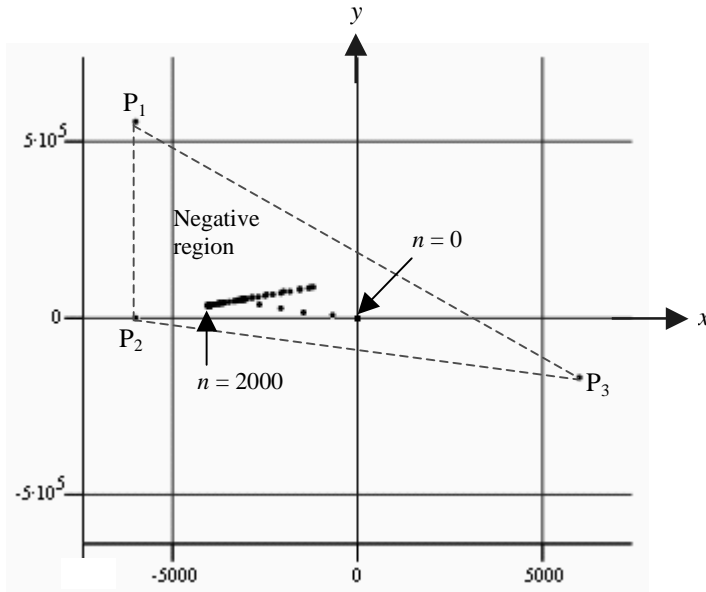


**Figure 6.11** – Location of the state  $(x, y)$  for  $n = 0$  to  $n = 2000$  at an interval of 10 time-steps.

## 6.6 End Notes

The theorems in Section 6.2 are useful. They overcome the limitations of Von-Neumann approach, which result in the CFL Criterion. First and foremost, they can be used to determine and ensure the stability of Yee's FDTD model for microwave circuit or high-speed PCB with the following conditions: (1) Variable and nonlinear dielectric constant. (2) Including the effect of PEC boundary. (3) Containing linear and nonlinear lumped elements. In applying Theorem 6.3, the only requirement for permittivity  $\epsilon$  is that it must be positive for all E field components while the requirement for permeability  $\mu$  is that it must be equal to  $\mu_0$  for all H field components.

Secondly, the conditions imposed on  $\epsilon_{r(i,j,k)}$ ,  $J_{r(i,j,k)}^{n+\frac{1}{2}}$  and  $P_d$  in Lemma 6.2 and Theorem 6.3 can be used as a test to check whether the FDTD formulation of a lumped element is proper. For a new lumped element, we can write its E field update equation

in the Canonical FDTD Form, determine the equivalent current density and compute its elemental dissipation  $\frac{1}{2} \left( E_{z(i,j,k)}^{n+1} + E_{z(i,j,k)}^n \right) J_{z(i,j,k)}^{n+\frac{1}{2}}$  against all possible combinations of dependent field components as shown in Section 6.3. As long as the elemental dissipation is greater or equal to zero and  $\epsilon_{r(i,j,k)} > 0$ , we know that the formulation is proper and will not contribute to instability of the model.

The Von-Neumann and other linear approaches cannot be used to analyze stability of the system under the above conditions of (1)-(3), and traditionally rule-of-thumbs are used to ensure that the FDTD model is stable (Chapter 2, Strikwerda 1989). In addition, the approach presented here can also be extended to include:

- Variable and nonlinear permeability.
- Non-uniform cell size.
- Dispersive elements and lumped inductors.
- Absorbing boundary condition.

The first and second extension can be carried out by writing  $\mu = \mu_{r(i,j,k)}$  and reformulating the condition for  $V^n$  to be positive definite. The third extension can be carried out by implementing a monitoring algorithm much like Figure 6.2. The details of the fourth extension are shown in Appendix 6. It is shown how replacing the PEC with absorbing boundary condition employing mathematical interpolation such as Mur's ABC would not affect the stability of the model. The proof in Appendix 6 is very useful as it can be applied to any absorbing boundary condition that uses mathematical approach. The fourth extension can also be achieved by introducing a few layers of cells with electric conductivity before the PEC boundary. A better approach would be to introduce magnetic conductivity and magnetic current in addition to electric conductivity. Then formulate an absorbing boundary condition (ABC) based on Perfectly Matched Layer (PML) method (Berenger 1994, Taflove 1995). Similar procedures as in the previous sections can be used to derive extended theorem incorporating magnetic loss of  $\frac{1}{2} \left( H_{r(i,j,k)}^{n+\frac{1}{2}} + H_{r(i,j,k)}^{n-\frac{1}{2}} \right) M_{r(i,j,k)}^n$ , where  $M_{r(i,j,k)}^n$  is the

corresponding magnetic current. The method does have some disadvantages. It will fail when there is update equations for either E or H field that cannot be written in the Canonical FDTD Form. Also the condition for  $\Delta t$  is slightly more rigid than CFL Criterion.